*J. Fluid Mech.* (1998), *vol.* 370, *pp.* 221–247. Printed in the United Kingdom



# Stagnation–saddle points and flow patterns in Stokes flow between contra-rotating cylinders

By P. H. GASKELL[1], M. D. SAVAGE[2] AND H. M. THOMPSON[1]

[1]School of Mechanical Engineering, The University of Leeds, Leeds LS2 9JT, UK
[2]Department of Physics and Astronomy, The University of Leeds, Leeds, LS2 9JT, UK

(Received 28 April 1997 and in revised form 6 April 1998)

The steady flow is considered of a Newtonian fluid, of viscosity $\mu$, between contra-rotating cylinders with peripheral speeds $U_1$ and $U_2$. The two-dimensional velocity field is determined correct to $O(H_0/2R)^{1/2}$, where $2H_0$ is the minimum separation of the cylinders and $R$ an 'averaged' cylinder radius. For flooded/moderately starved inlets there are two stagnation–saddle points, located symmetrically about the nip, and separated by quasi-unidirectional flow. These stagnation–saddle points are shown to divide the gap in the ratio $U_1 : U_2$ and arise at $|X| = A$ where the semi-gap thickness is $H(A)$ and the streamwise pressure gradient is given by $dP/dX = \mu(U_1+U_2)/H^2(A)$. Several additional results then follow.

(i) The effect of non-dimensional flow rate, $\lambda$: $A^2 = 2RH_0(3\lambda - 1)$ and so the stagnation–saddle points are absent for $\lambda < 1/3$, coincident for $\lambda = 1/3$ and separated for $\lambda > 1/3$.

(ii) The effect of speed ratio, $S = U_1/U_2$: stagnation–saddle points are located on the boundary of recirculating flow and are coincident with its leading edge only for symmetric flows ($S = 1$). The effect of unequal cylinder speeds is to introduce a displacement that increases to a maximum of $O(RH_0)^{1/2}$ as $S \to 0$.

Five distinct flow patterns are identified between the nip and the downstream meniscus. Three are asymmetric flows with a transfer jet conveying fluid across the recirculation region and arising due to unequal cylinder speeds, unequal cylinder radii, gravity or a combination of these. Two others exhibit no transfer jet and correspond to symmetric ($S = 1$) or asymmetric ($S \neq 1$) flow with two asymmetric effects in balance. Film splitting at the downstream stagnation–saddle point produces uniform films, attached to the cylinders, of thickness $H_1$ and $H_2$, where

$$\frac{H_1}{H_2} = \frac{S(S+3)}{3S+1},$$

provided the flux in the transfer jet is assumed to be negligible.

(iii) The effect of capillary number, $Ca$: as $Ca$ is increased the downstream meniscus advances towards the nip and the stagnation–saddle point either attaches itself to the meniscus or disappears via a saddle–node annihilation according to the flow topology.

Theoretical predictions are supported by experimental data and finite element computations.

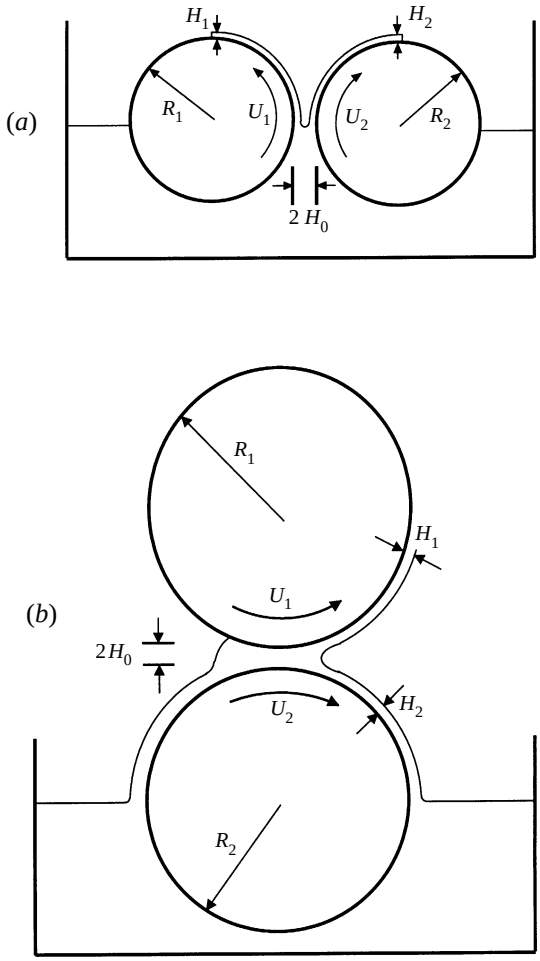


FIGURE 1. Film-splitting between contra-rotating cylinders aligned (*a*) horizontally; (*b*) vertically.

## 1. Introduction

Viscous flow in a cross-sectional plane between long cylinders has been researched extensively, particularly with regard to applications such as fixed-gap roll coating. In forward roll coating, figure 1(*a,b*), cylinders, either horizontally or vertically aligned, having radii $R_1$, $R_2$ move with peripheral speeds $U_1$, $U_2$, and hence speed ratio $S = U_1/U_2$, in the same direction (contra-rotating) through the nip region where the minimum cylinder separation is $2H_0$. Experimental, analytical and computational investigations for fluids that are Newtonian with viscosity $\mu$ and surface tension $\sigma$, have sought to identify the governing parameters and determine the key features and flow variables. These include flow rate, $\lambda$, film thicknesses, $H_1$, $H_2$, the velocity and pressure fields, $\boldsymbol{U} = (U, W)$, $P$, location of the downstream free surface (meniscus) and stagnation points which identify the onset of recirculating flow.

The presence of recirculating flow immediately adjacent to the downstream meniscus was first reported by Pitts & Greiller (1961), substantiated by Schneider (1962) and Van de Bergh (1974) and later captured on video by Malone (1992). Also Ruschak (1982) predicted and Malone (1992) confirmed that, as capillary number, $Ca = \mu U_2/\sigma$, increases, the extent of this reverse flow region contracts and disappears for $Ca \gtrsim 1$.

Several authors have measured flow rate: Pitts & Greiller (1961), Hintermaier & White (1965), Greener & Middleman (1975). For cylinders of equal speed, Benkreira, Edwards & Wilkinson (1981) obtained a maximum non-dimensional flow rate $\lambda = 1.31$ which showed little variation with $Ca$. This result was confirmed by Malone (1992) who also showed that the location of the stagnation point marking the onset of the recirculation region exhibited no apparent variation. In contrast, the position and shape of the meniscus is highly dependent on $Ca$, being closest to the nip when $Ca > 1$ and receding away from the nip as $Ca$ decreases (Coyle, Macosko & Scriven 1986; Decré, Gailly & Buchlin 1995).

For the case $S = 1$, Greener & Middleman (1975, 1979) formulated a mathematical model based on lubrication theory which gave rise to the Reynolds equation for pressure. They considered a semi-infinite domain which terminated downstream of the nip at a stagnation point where not only velocity but also velocity gradient is zero due to symmetry. The conditions $U = \partial U/\partial Z = 0$, known as the Prandtl–Hopkins conditions, apply to symmetric flows and also, with one cylinder at rest, they locate the point at which the flow separates from the stationary surface. Subsequently, Savage (1982) extended the model to the general case of $S \neq 1$ by postulating that the Prandtl–Hopkins conditions remain valid and locate the onset of the recirculation region as both a stagnation point and a point of flow separation. This is usually referred to as the 'separation hypothesis' which gives rise to a prediction for film thicknesses ratio, $H_1/H_2$, in terms of $S$:

$$\frac{H_1}{H_2} = S^{1/2}.$$

The limitations of mathematical models based on lubrication theory were only too evident to the above authors, as indeed they were to Taylor (1963) who pointed out that flows found in journal bearings and between contra-rotating cylinders consist of two distinct regions: a region where the flow is adequately described by lubrication theory and a region near the meniscus where the flow is fully two-dimensional. For symmetric flows Ruschak (1982) analysed the two-dimensional problem by means of the method of matched asymptotic expansions. Essentially the inner problem required a two-dimensional solution of the Navier–Stokes equations in the vicinity of the meniscus which was then matched onto an outer, lubrication solution. Calculations revealed the importance of $Ca$ in locating both the position of the meniscus and the ratio, $H_1/H(c)$, of the film thickness to half-gap width at the meniscus. This latter parameter arises from matching the pressure gradients of the inner and outer solutions. In fact its significance in specifying the pressure gradient at the meniscus was first appreciated by Coyne & Elrod (1970). They performed an approximate analysis of the free-surface flow from the meniscus to uniform flow at infinity obtaining results almost identical with those of Ruschak (1982).

Coyle *et al.* (1986) generalized Ruschak's (1982) matched asymptotic analysis to the asymmetric case with $S \neq 1$ and in both cases the inner problem required a numerical solution obtained using finite elements (FEs). A FE method for solving the Navier–Stokes equations for the full velocity and pressure fields subject to appropriate boundary conditions, also emerged in parallel (see Kistler & Scriven 1983). Coyle *et al.*'s (1986) numerical results for film thickness ratio expressed $H_1/H_2$ in terms of $S$ via a power law

$$\frac{H_1}{H_2} = S^{0.65}, \quad S \in (0.1, 10.0),$$

where the exponent 0.65 is identical to that found by Benkreira *et al.* (1981) from experimental data over the same range of $S$.

Theoretical predictions for $H_1/H_2$ from the separation hypothesis are clearly out of line with results from experimental and computational analysis. This provides motivation for the present work since one would expect lubrication theory, despite its obvious limitations, to predict accurately the onset of reverse flow and hence the uniform film thickness on each cylinder. The fact that this is not so casts considerable doubt on the validity of the Prandtl–Hopkins conditions. Though these conditions hold in two special cases it is now clear that the error is in assuming them to be generally valid. Indeed there is no physical basis for imposing the condition $\partial U/\partial Z = 0$ for $S > 0$, $S \neq 1$. Hence there is no alternative but to consider the two-dimensional velocity field and impose conditions on both components of velocity, $\boldsymbol{U} = (U, W) = (0, 0)$, to determine the location of the stagnation point which is also a saddle point located on the boundary of recirculating flow.

Two-dimensional flow between rotating cylinders has been investigated by a number of previous authors; Jeffery (1922) analysed Stokes flow between fully submerged contra-rotating cylinders using bi-polar coordinates. Ballal & Rivlin (1976) also used a bi-polar coordinate system to solve for the flow between eccentric cylinders, either with or without inertia. They reported the existence of a rich variety of streamline patterns and established a number of conditions under which stagnation points, separation points and eddies can exist. Flow asymmetries when $S \neq 1$ were investigated by Coyle *et al.* (1986) who predicted via FE computations the existence in the downstream recirculation region, figure 2(*d*), of a transfer jet or 'snake' by which flux is transferred from the slow to the faster moving cylinder. Recent experiments by Gaskell, Savage & Walker (1998), using dye injection coupled with a high-speed video to examine the flow in the nip region between two half-submerged cylinders, figure 1(*a*), have confirmed this transfer mechanism. They also identified others due to unequal cylinder radii and the effect of gravity. In each case, however, the transfer jet is a weak, secondary flow with only a very small flux transferred.

Wicks *et al.* (1995) used a dynamical systems approach supported by experiment and numerical simulations to analyse the loss of symmetry in the downstream recirculation region and identified two distinct flow topologies. They referred to symmetric flow ($S = 1$) as a 'joint eddy topology' since the two eddies share a common streamline and are attached to the free surface. In contrast, asymmetric flow is referred to as a 'disjoint eddy topology' since the two eddies are separated by a transfer jet with one now detached from the free surface. They showed the disjoint eddy topology to be generic if any source of asymmetry is present.

In the mathematical model, §2, the two-dimensional velocity field and the location of the stagnation–saddle points are determined correct to $O(H_0/2R)^{1/2}$. This enables a series of results to be established analytically with new and unexpected predictions for both the location of the stagnation–saddle points and the film thickness ratio. In turn, these predictions initiated further experimental and computational investigations. In §3 the effects of $\lambda$, $S$ and $Ca$ on the location of stagnation–saddle points are considered. Specific aims include (i) locating the onset of recirculating flow in relation to a stagnation–saddle point and showing that the two are only coincident in the case of symmetric flow; (ii) revealing the five basic flow patterns which can arise in the recirculation region with topologies of the 'joint eddy' or 'disjoint eddy' type; (iii) investigating the various mechanisms by which transfer jets arise, and in some cases cancel each other out, namely unequal cylinder speeds, unequal cylinder radii, gravity across the gap and 'asymmetric inlet feeding'. Finally in §4 the thicknesses of

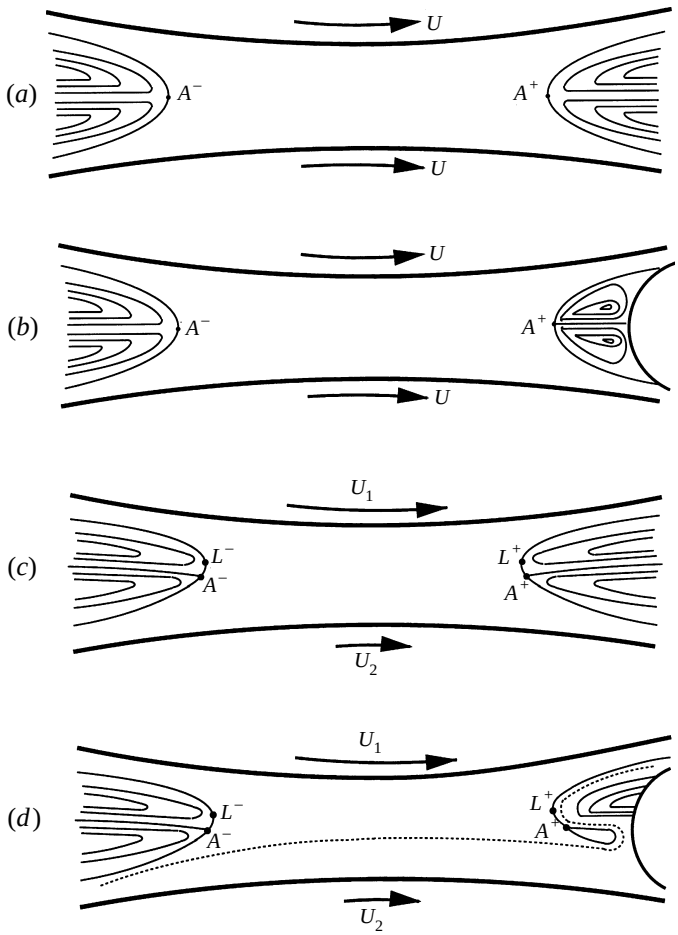


FIGURE 2. Schematic of symmetric flow $S = 1$ and asymmetric flow $S \neq 1$ between fully submerged cylinders (*a*,*c*) and in the presence of a downstream meniscus (*b*,*d*). $A^+$ and $A^-$ are stagnation–saddle points; $L^+$ and $L^-$the leading edges of the recirculations. A transfer jet, indicated by a dotted line, is shown in the downstream recirculation region in (*d*).

the uniform films attached to the cylinders are calculated and the film thickness ratio is derived as a simple algebraic function of $S$. Theoretical predictions are compared with experimental data and FE computations.

## 2. Mathematical model and solution

Two-dimensional flow between contra-rotating cylinders is illustrated schematically in figure 2(*a–d*). In each case the inlet is assumed to be flooded/moderately starved so that a region of quasi-unidirectional flow is followed by recirculations extending either to infinity or to a meniscus. When the cylinders have unequal speeds, a key feature within the recirculating flow, downstream of the nip, is the presence of a weak transfer jet transferring fluid from the slower to the faster moving cylinder, figure 2(*d*). Asymmetric transfer jets also arise due to unequal cylinder radii and gravity, and all involve a stagnation–saddle point, $A^+$, with a homoclinic orbit around which the jet meanders. Hence one aim here is to locate stagnation–saddle points, by means of an

appropriate set of equations, correct to $O(\delta)$ where $\delta^2 = H_0/2R$ is assumed small and $R$ is an averaged cylinder radius defined by $2/R = (1/R_1 + 1/R_2)$.

The origin of $(X, Z)$ coordinates is taken to lie in the mid-plane of the nip, a distance $H_0$ from either cylinder, so that the cylinder surfaces are given by $H_1(X) = H_0 + X^2/2R_1$ and $H_2(X) = H_0 + X^2/2R_2$, respectively. The flow is assumed to be incompressible and described by Stokes' equations

$$\left.\begin{aligned} \frac{\partial P}{\partial X} &= \mu\left(\frac{\partial^2 U}{\partial X^2} + \frac{\partial^2 U}{\partial Z^2}\right), \\ \frac{\partial P}{\partial Z} &= \mu\left(\frac{\partial^2 W}{\partial X^2} + \frac{\partial^2 W}{\partial Z^2}\right) - \rho g, \end{aligned}\right\} \tag{2.1}$$

$$0 = \frac{\partial U}{\partial X} + \frac{\partial W}{\partial Z}. \tag{2.2}$$

Equations (2.1) and (2.2) are non-dimensionalized by introducing new variables $x$, $z$, $u$, $w$ and $p$ defined by

$$x = \frac{X}{(2RH_0)^{1/2}}, \quad z = \frac{Z}{H_0}, \quad u = \frac{U}{U_2}, \quad w = \frac{W}{\delta U_2}, \quad p = \frac{H_0\delta}{\mu U_2}P, \tag{2.3}$$

giving

$$\left.\begin{aligned} \frac{\partial p}{\partial x} &= \frac{\partial^2 u}{\partial z^2} + \delta^2\frac{\partial^2 u}{\partial x^2}, \\ \frac{\partial p}{\partial z} &= \delta^2\frac{\partial^2 w}{\partial z^2} + \delta^4\frac{\partial^2 w}{\partial x^2} - St, \\ 0 &= \left(\frac{\partial u}{\partial x} + \frac{\partial w}{\partial z}\right), \end{aligned}\right\} \tag{2.4}$$

where $St = \rho g H_0^2/\mu U_2$ is the Stokes number. Neglecting gravity, a solution for $u$, $w$, and $p$ in powers of $\delta^2$ yields the lubrication equations at lowest order

$$\frac{\partial p}{\partial x} = \frac{\partial^2 u}{\partial z^2}, \quad \frac{\partial p}{\partial z} = 0 \Rightarrow p = p(x), \tag{2.5}$$

$$\frac{\partial u}{\partial x} + \frac{\partial w}{\partial z} = 0. \tag{2.6}$$

To determine $u$, $w$ and locate the stagnation–saddle points attention is restricted to the case of equal cylinder radii since the key results are identical to the general case where the analysis is much more intricate – see the Appendix. With $R_1 = R_2 = R$ the cylinder surfaces are given by

$$Z = \pm H(X), \quad \text{i.e.} \quad z = \pm\eta(x) = \pm(1 + x^2). \tag{2.7}$$

Hence the solution for $u(x, z)$ satisfying $u = 1$ on $z = -\eta(x)$ and $u = S$ on $z = +\eta(x)$ is

$$u(x, z) = \frac{p_x}{2}(z^2 - \eta^2) + \left(\frac{S-1}{2}\right)\frac{z}{\eta} + \left(\frac{S+1}{2}\right), \tag{2.8}$$

where $p_x = \mathrm{d}p/\mathrm{d}x$.

The $Z$-component of velocity has to satisfy $W = U_1(\mathrm{d}H/\mathrm{d}X)$ on $Z = H(X)$ and $W = -U_2(\mathrm{d}H/\mathrm{d}X)$ on $Z = -H(X)$, that is

$$\left.\begin{aligned} w &= S\eta_x \quad \text{on} \quad z = +\eta(x), \\ w &= -\eta_x \quad \text{on} \quad z = -\eta(x), \end{aligned}\right\} \tag{2.9}$$

where $\eta_x = (\mathrm{d}\eta/\mathrm{d}x)$. The solution for $w(x, z)$ is therefore

$$w(x,z) = S\eta_x - \frac{p_{xx}}{2}\left(\frac{z^3}{3} - z\eta^2 + \frac{2\eta^3}{3}\right) + \frac{p_x}{2}\eta\eta_x(z-\eta) + \frac{(S-1)\eta_x}{4\eta^2}(z^2-\eta^2). \tag{2.10}$$

Since the flow is steady the flux, $Q$, is constant. Hence

$$Q = \int_{-H}^{+H} U\mathrm{d}Z = U_2H_0\int_{-\eta}^{+\eta} u(x,z)\mathrm{d}z, \tag{2.11}$$

reduces to the non-dimensional Reynolds equation

$$\frac{\mathrm{d}p}{\mathrm{d}x} = \frac{3}{2}\left[\frac{(S+1)}{\eta^2} - \frac{Q}{U_2H_0\eta^3}\right]. \tag{2.12}$$

Isolating $Q$ and differentiating with respect to $x$ yields an expression for $(\mathrm{d}^2p/\mathrm{d}x^2) = p_{xx}$ giving rise to a two-dimensional velocity field in terms of $p_x$ and correct to $O(\delta)$:

$$\left.\begin{aligned} u(x,z) &= \frac{p_x}{2}\eta^2\left[\left(\frac{z}{\eta}\right)^2 - 1\right] + \left(\frac{S-1}{2}\right)\frac{z}{\eta} + \left(\frac{S+1}{2}\right), \\ w(x,z) &= \eta_x\left\{\frac{1}{2}\left[p_x\eta^2 - \left(\frac{1+S}{2}\right)\right]\left[\left(\frac{z}{\eta}\right)^3 - 3\left(\frac{z}{\eta}\right) + 2\right]\right\} \\ &\quad + \eta_x\left\{p_x\eta^2\left(\frac{z}{\eta} - 1\right) + \left(\frac{S-1}{4}\right)\left[\left(\frac{z}{\eta}\right)^2 - 1\right] + S\right\}. \end{aligned}\right\} \tag{2.13}$$

If the coordinates of a stagnation point are denoted by $(X, Z) = (A, \theta H(A))$, that is

$$x = a, \quad \frac{z}{\eta(a)} = \theta, \tag{2.14}$$

and if $\alpha$ is introduced where

$$\alpha = \frac{\eta^2(a)p_x(a)}{(1+S)}, \tag{2.15}$$

then $u = w = 0$ gives two sets of solutions for $\alpha$ and $\theta$, namely

$$\left.\begin{aligned} \alpha(\theta^2-1) + \left(\frac{S-1}{S+1}\right)\theta + 1 &= 0, \\ \eta_x &= 0, \end{aligned}\right\} \tag{2.16}$$

and

$$\left.\begin{aligned} \alpha(\theta^2-1) + \left(\frac{S-1}{S+1}\right)\theta + 1 &= 0, \\ 2\alpha\theta(\theta^2-1) + \left(\frac{S-1}{S+1}\right)(\theta^2-1) + \frac{4S}{1+S} - (\theta^3 - 3\theta + 2) &= 0. \end{aligned}\right\} \tag{2.17}$$

### 2.1. *Stagnation points in the nip* ($X = 0$)

Here $\eta = 1$, $\eta_x = 0$ and via (2.12)

$$\frac{\mathrm{d}p}{\mathrm{d}x} = \frac{3(1+S)}{2}(1-\lambda), \tag{2.18}$$

where $\lambda$ is a non-dimensional flow rate

$$\lambda = \frac{Q}{(U_1+U_2)H_0}. \tag{2.19}$$

Hence equations (2.16) give a quadratic for $\theta$:

$$(1-\lambda)\theta^2 + \frac{2}{3}\left(\frac{S-1}{S+1}\right)\theta + (\lambda - \tfrac{1}{3}) = 0, \tag{2.20}$$

with solutions

$$\theta = \frac{-\frac{2}{3}\left(\frac{S-1}{S+1}\right) \pm \left[\frac{4}{9}\left(\frac{S-1}{S+1}\right)^2 - 4(1-\lambda)(\lambda-\frac{1}{3})\right]^{1/2}}{2(1-\lambda)}. \tag{2.21}$$

Real solutions exist provided

$$\left(\frac{S-1}{S+1}\right)^2 > (3-3\lambda)(3\lambda-1), \quad (\lambda - \tfrac{2}{3})^2 > \frac{4S}{9(1+S)^2}, \tag{2.22}$$

and those corresponding to $|\theta| \leqslant 1$ are given by

$$\lambda < \bar{\lambda} = \frac{2}{3}\left[1 - \frac{S^{1/2}}{(1+S)}\right]. \tag{2.23}$$

Stagnation points appear in the nip only for small flow rates, less than a critical value $\bar{\lambda}$ which depends on $S$. In fact $\bar{\lambda}$ is a minimum when $S = 1$, $\bar{\lambda}(1) = 1/3$ and increases towards $\bar{\lambda} = 2/3$ as $S \to 0$ and $S \to \infty$, figure 3. For a given $S$ and $\lambda = \bar{\lambda}(S)$ a stagnation point arises at

$$(x, z) = \left(0, \frac{(1-S)}{3(1+S)(1-\lambda)}\right) = \left(0, \frac{(1-S^{1/2})}{(1+S^{1/2})}\right), \tag{2.24}$$

and subsequently two stagnation points separate across the gap as $\lambda$ decreases. For such flow rates, $\lambda \leqslant \bar{\lambda}(S)$, the pressure gradient (2.12) is everywhere positive which corresponds to the meniscus coating regime, Gaskell *et al.* (1995*a*). However, here attention is focused on the complementary flow regime in which $\lambda > \bar{\lambda}(S)$, inlets are flooded/moderately starved and there are no stagnation points in the nip.

### 2.2. *Stagnation points beyond the nip* ($|X| = A > 0$)

The solution of equations (2.17) will locate those stagnation points lying outside the nip. Substituting for $\alpha(\theta^2 - 1)$ yields a cubic in $\theta$:

$$(1+S)\theta^3 - (1-S)\theta^2 - (1+S)\theta + (1-S) = 0, \tag{2.25}$$

with solutions

$$\theta^2 = 1 \quad \text{and} \quad \theta = \frac{1-S}{1+S}. \tag{2.26}$$

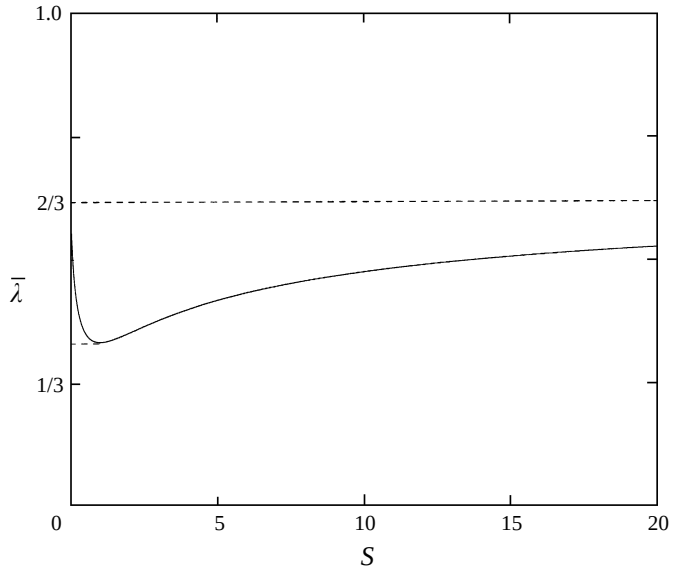


FIGURE 3. Critical flow rate $\overline{\lambda}$ as a function of $S$, equation (2.23), for the emergence of a stagnation point in the nip.

Solutions $\theta = 1$, $\theta = -1$ correspond to $S = 0$ and $S = \infty$ respectively. This is the case of a stationary cylinder, every point of which is a stagnation point, and the solution of equations (2.17) for $\alpha$ (where it appears with coefficient $(\theta^2 - 1)$) is arbitrary.

Of particular interest is the solution $\theta = (1 - S)/(1 + S)$, $(S > 0)$ which via (2.17) gives $\alpha = 1$ and therefore

$$p_x(a) = \frac{(1 + S)}{\eta^2(a)}. \tag{2.27}$$

Hence a stagnation point with coordinates $(X, Z) = (A, \theta H(A))$ arises where the streamwise pressure gradient is given by

$$\frac{\mathrm{d}P}{\mathrm{d}X} = \mu \frac{(U_1 + U_2)}{H^2(A)}, \tag{2.28}$$

and divides the gap (of width $2H(A)$) in the ratio

$$\frac{1 - \theta}{1 + \theta} = S = \frac{U_1}{U_2}. \tag{2.29}$$

The $X$-coordinate of the stagnation point, $X = A$, and the semi-gap thickness, $H(A)$, can be expressed in terms of $\lambda$ by using Reynolds' equation in the form

$$\frac{\mathrm{d}P}{\mathrm{d}X} = \frac{3\mu(U_1 + U_2)}{2H^2(X)} \left[1 - \frac{\lambda H_0}{H(X)}\right]. \tag{2.30}$$

Evaluating (2.30) at $X = A$ and equating with (2.27) gives the position $X = A$ and the semi-gap thickness $H(A)$:

$$A^2 = (2RH_0)(3\lambda - 1); \quad H(A) = 3\lambda H_0. \tag{2.31}$$

As indicated in the Appendix, results (2.29) and (2.31) are quite general and apply for cylinders of any radii and any $S > 0$. Expression (2.31) implies that for $\lambda > 1/3$ there

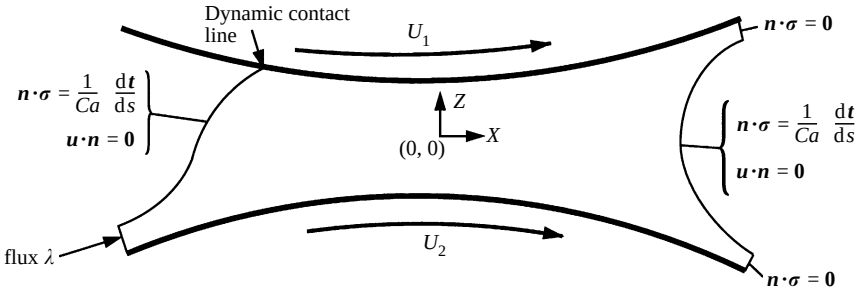


FIGURE 4. Full boundary value problem, solution domain and boundary conditions.

are possibly two stagnation–saddle points located either side of the nip at $X = \pm A$, figure 2. In practice one of these points may be absent since either the upstream or downstream meniscus may advance close to the nip depending upon the value of $\lambda$ or $Ca$ – see §3.1.

## 3. Stagnation–saddle points

### 3.1. *Effect of flow rate*

Figure 4 illustrates the full FE solution domain and boundary conditions – for further details see Gaskell *et al.* (1995*a,b*). However, it is common practice in the case of flooded inlets to solve in the downstream region only by replacing the upstream flow with lubrication conditions imposed at $X = 0$ (Coyle *et al.* 1986; Thompson 1992):

$$\left.\begin{aligned} U = U(0, Z, \lambda), \quad |Z| \leqslant H_0, \\ W = W(0, Z, \lambda) = 0. \end{aligned}\right\} \tag{3.1}$$

The position and separation of the two stagnation–saddle points is given by expression (2.31) as a function of $\lambda$. Both points approach the origin as $\lambda \to \frac{1}{3}$ ($\lambda > \frac{1}{3}$) and coalesce when $\lambda = \frac{1}{3}$. This analytical prediction is compared with the results of FE computations which make use of a stagnation point searching and classification algorithm for free surface flows devised by Gaskell *et al.* (1995*b*). The first case considered is that of symmetric flow, figure 2(*a,b*). For $R/H_0 = 100$, $Ca = 0.02$ and large to moderate flow rates figure 5(*a–c*) shows flow between the nip and the downstream meniscus.

For lower flow rates, figure 6(*a,b*) where the full flow field is revealed, $A^+$ is much closer to the nip. However, $A^-$ is absent due to the position of the upstream meniscus being close to the nip and there are no upstream recirculations present. That lubrication theory can locate $A^+$ and $A^-$ accurately is apparent from table 1 where theoretical predictions via (2.31) are compared with computational results for $S = 1$ (and $S = 4$) over a range of flow rates $\lambda \in (1/3, \lambda_{max})$.

### 3.2. *Effect of speed ratio*

Asymmetric flow for $S = 4$, $R/H_0 = 100$ and $Ca = 0.005$ is shown in figure 7(*a–c*). Computational results given in table 1 confirm that $X = A$, the $X$-coordinate of $A^+$, depends on $\lambda$ but is effectively independent of $S$. Key features in figure 7 include (i) a transfer jet in the recirculation region conveying fluid from the slower to the faster moving cylinder – see §3.4 – and (ii) a stagnation–saddle point $A^+$ that is no longer coincident with $L^+$ at the onset of recirculating flow, figure 2(*c,d*).

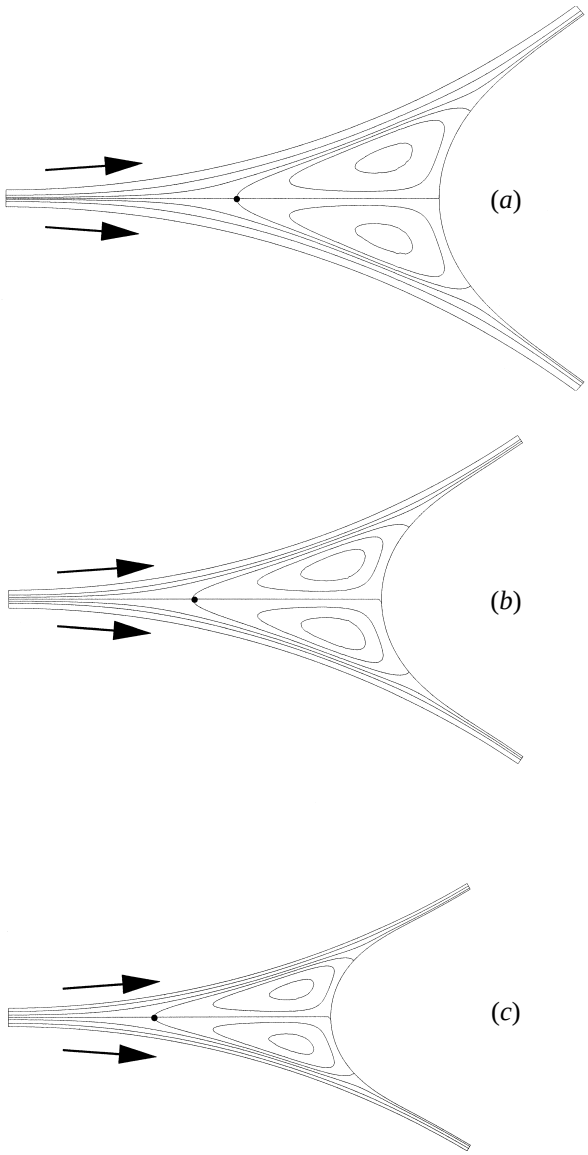


FIGURE 5. Downstream-only FE solutions for $S = 1$, $Ca = 0.02$, $R/H_0 = 100$, $R_1/R_2 = 1$ and $St = 0$ showing the displacement of $A^+$ (indicated by •) towards the nip as $\lambda$ is reduced: (*a*) $\lambda_{max} = 1.379$; (*b*) $\lambda = 1.000$; (*c*) $\lambda = 0.750$.

In addition figure 8 shows a close-up of flow around the leading edge of the recirculations. Unlike the symmetric case ($U_1 = U_2$), there is no flow separation at $L^+$ (or $L^-$) when cylinder speeds are unequal. Fluid cannot flow around both sides of $L^+$ since it is blocked on one side by the presence of the saddle at $A^+$.

*Locating the onset of recirculations*

Clearly $u = 0$ at $L^+$ but $\partial u/\partial z$ is unknown and so the problem is how to locate $L^+$ when $S \neq 1$! In fact, despite the absence of flow separation in the usual sense when $S \neq 1$, there is a point $P^H$ – just upstream of $L^+$ – where the Prandtl–

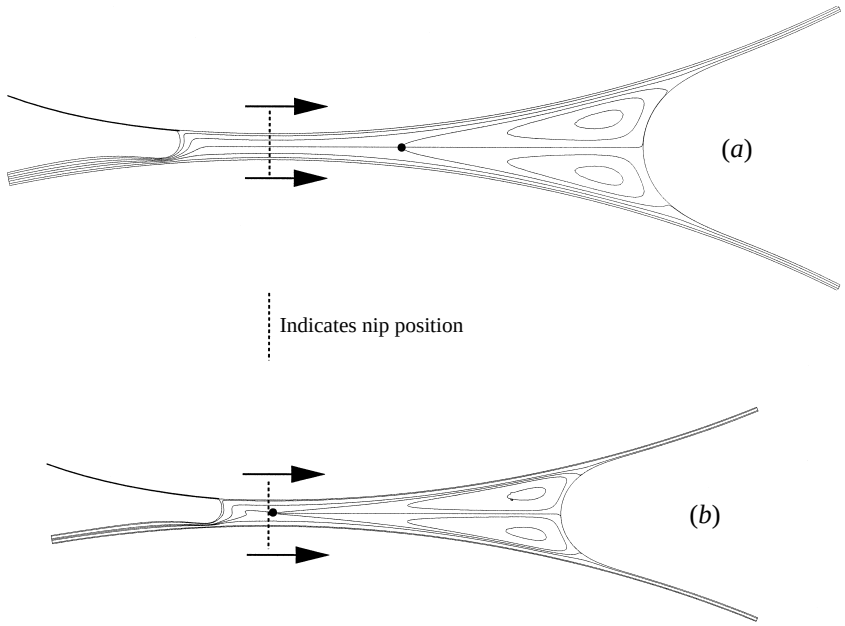


FIGURE 6. FE solutions for the full domain with $S = 1$, $Ca = 0.02$, $R/H_0 = 100$, $R_1/R_2 = 1$ and $St = 0$ for two values of $\lambda$: (*a*) 0.500; (*b*) 0.333. $A^+$ is indicated by •.

| | Stagnation point location, $X = A$ | | |
|---|---|---|---|
| $\lambda$ | Analytical | Computational ($S = 1$, $Ca = 0.02$) | Computational ($S = 4$, $Ca = 0.005$) |
| 1.30 | 24.083 | 24.253 | 24.181 |
| 1.20 | 22.804 | 22.961 | 22.891 |
| 1.10 | 21.448 | 21.588 | 21.519 |
| 1.00 | 20.000 | 20.124 | 20.068 |
| 0.90 | 18.439 | 18.548 | 18.498 |
| 0.80 | 16.733 | 16.829 | 16.788 |
| 0.70 | 14.832 | 14.915 | 14.923 |
| 0.60 | 12.649 | 12.718 | 12.711 |
| 0.50 | 10.000 | 10.055 | 10.071 |
| 0.40 | 6.325 | 6.367 | 6.409 |
| 0.38 | 5.292 | 5.330 | 5.390 |
| 0.36 | 4.000 | 4.023 | 4.116 |
| 0.34 | 2.000 | 2.110 | 2.068 |

TABLE 1. Comparison between analytical and numerical predictions of stagnation–saddle point location $X = A$, as a function of $\lambda$, for $S = 1$, $Ca = 0.02$ and $S = 4$, $Ca = 0.005$.

Hopkins conditions do hold. This can be inferred by considering the three streamlines approaching $A^+$ shown in figure 8.

The one closest to $L^+$ is typical of those that 'double-back' – having two turning points where $u = 0$ and a point of minimum velocity, $\partial u/\partial z = 0$ where $u < 0$. The one passing through $P^H$ is a dividing streamline on which $u > 0$ except at the point, $P^H$, where $u = 0$ and $\partial u/\partial z = 0$. The streamline furthest from $L^+$ is typical of those on which $u > 0$, i.e. locally there are no points where $u = 0$. So the dividing streamline can be regarded as the limiting case of a bundle of streamlines as the minimum

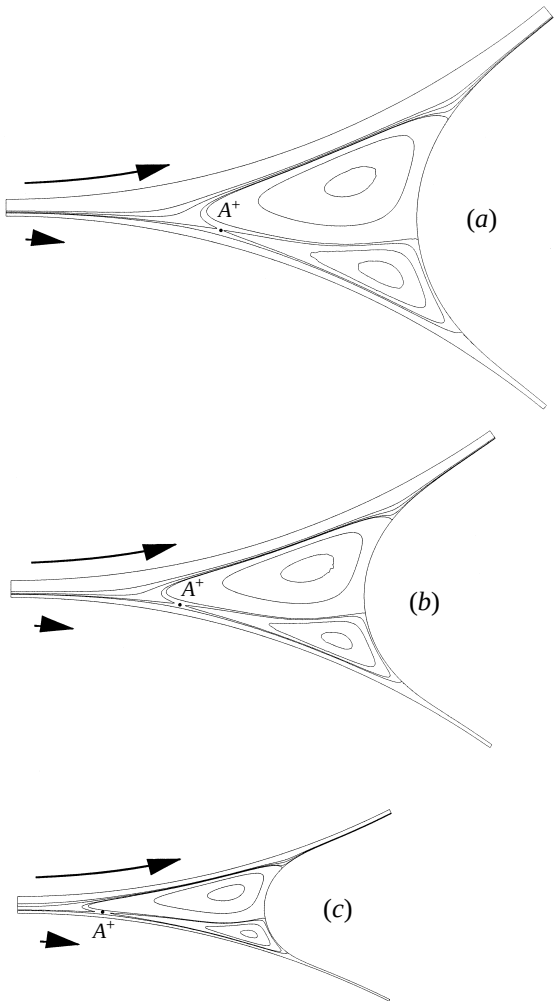


FIGURE 7. Downstream-only FE solutions for $S = 4$, $Ca = 0.005$, $R/H_0 = 100$, $R_1/R_2 = 1$ and $St = 0$ showing the displacement of $A^+$ (indicated by •) towards the nip as $\lambda$ is reduced: (*a*) $\lambda_{max} = 1.402$; (*b*) $\lambda = 1.000$; (*c*) $\lambda = 0.500$.

velocity diminishes and becomes zero. The point $P^H$ is positioned close to $L^+$. They have approximately the same $Z$-coordinate and their $X$-coordinates are separated by a small distance ($\ll H_0$) so as to permit streamlines which double-back to pass between them. The following conclusions can be drawn:

(i) At $P^H$ the Prandtl–Hopkins conditions apply yet it is not a separation point. Here, we refer to it as a 'Prandtl–Hopkins' point.

(ii) The position of $P^H$ provides an approximation to that of $L^+$, the onset of recirculations.

(iii) As $\lambda$ is reduced for a given $S$, $P^H$ approaches the nip as does its companion on the other side of the nip. When $\lambda = \bar{\lambda}$ the two points collide to produce a stagnation point (the birth of a saddle-node) at the location given by expression (2.24). Furthermore, FE computations confirm the presence in the nip of a saddle and a centre for $\lambda \in (1/3, \bar{\lambda})$, figure 9(*a–c*).

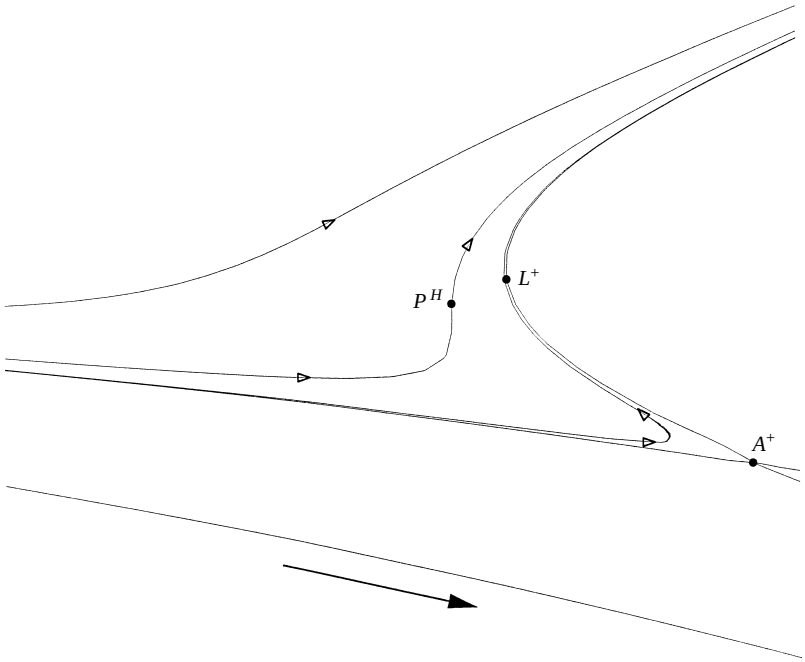


FIGURE 8. Three streamlines approaching $A^+$, for $S = 4.0$, $Ca = 0.005$, $R/H_0 = 100$, $R_1/R_2 = 1$ and $St = 0$, and flowing around $L^+$ the leading edge of the recirculation region. $P^H$ indicates where $u = \partial u/\partial z = 0$.

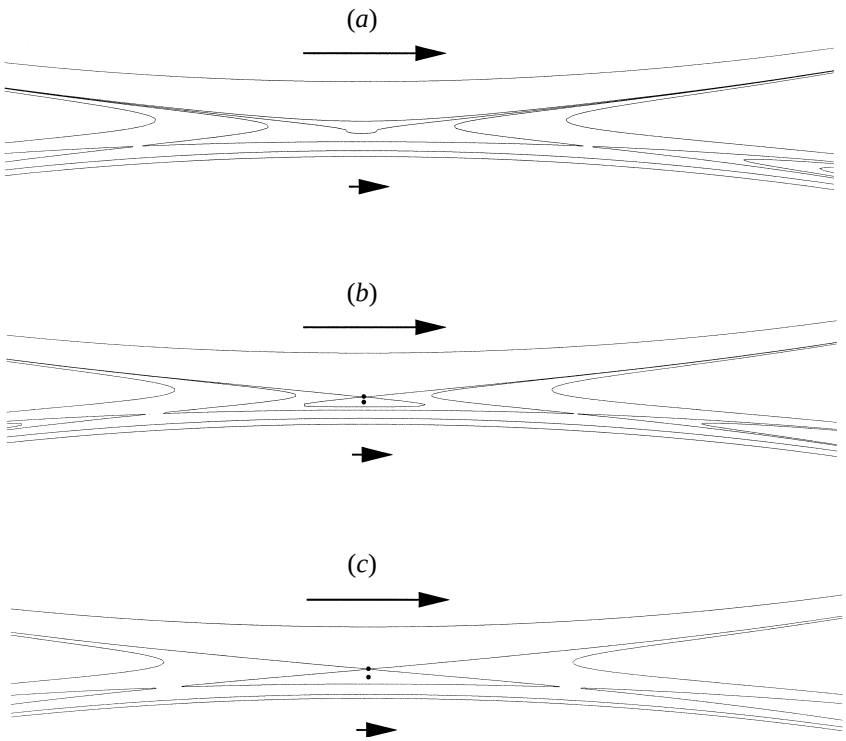


FIGURE 9. The emergence of stagnation points in the nip (a saddle and a centre, denoted by •) as flow rate is reduced for $S = 4.0$, $Ca = 0.01$, $R/H_0 = 100$, $R_1/R_2 = 1$ and $St = 0$: (*a*) $\lambda = 0.405$; (*b*) 0.394; (*c*) 0.386.

*Displacement of $L^+$ from $A^+$*

Analytically the displacement of a stagnation–saddle point from the leading edge of recirculating flow can be estimated to be of order $(RH_0)^{1/2}$ if a Couette–Poiseiulle velocity profile for $U(X,Z)$ is assumed, expression (2.8). Although the latter cannot describe the two-dimensional flow between $P^H$, $L^+$ and $A^+$ it has proved remarkably successful in locating $A^+$. This is perhaps due to $A^+$ being on the boundary of a region of flow that is effectively unidirectional and so we might expect (2.8) to do likewise for $P^H$.

If the coordinates of $P^H$ are $(L,\overline{Z})$ then imposing the Prandtl–Hopkins conditions, $u = \partial u/\partial z = 0$ gives the streamwise pressure gradient at $X = L$:

$$\frac{\mathrm{d}p}{\mathrm{d}x} = \mu\frac{[U_1^{1/2} + U_2^{1/2}]^2}{2H^2(L)}. \tag{3.2}$$

Hence

$$L^2 = \left[\frac{3\lambda(1+S)}{(1+S-S^{1/2})} - 2\right] RH_0, \quad \overline{Z} = \left(\frac{1-S^{1/2}}{1+S^{1/2}}\right) H(L), \tag{3.3}$$

and

$$\frac{(A-L)}{(2RH_0)^{1/2}} = (3\lambda-1)^{1/2} - \left(\frac{3\lambda(1+S)}{2(1+S-S^{1/2})} - 1\right)^{1/2}. \tag{3.4}$$

Taking $P^H$ as an approximation to $L^+$, then (3.4) shows that the displacement between $A^+$ and $L^+$ depends on both $\lambda$ and $S$ and increases as $S \to 0$ to a maximum

$$\frac{(A-L)}{(2RH_0)^{1/2}} = (3\lambda-1)^{1/2} - \left(\frac{3\lambda}{2} - 1\right)^{1/2}.$$

This is illustrated in figure 10 (*a–d*) which shows the effect of decreasing $S$ for a flow rate $\lambda \approx 1.3$. Indeed as $S$ is reduced from $S = 1$ the location of $A^+$ moves towards the slower cylinder whilst its $X$-coordinate remains effectively constant. The position of $L^+$ moves further upstream and the displacement $(A - L)$ increases as indicated by (3.4). Although (3.4) predicts the right trends, nevertheless it would be desirable to confirm its accuracy via the numerical solution. Unfortunately, confirmation of this numerically was not possible due to the interpolation functions employed in the FE calculations being of too low an order for the degree of accuracy required.

A further observation concerns the dependence on $S$ of the $Z$-coordinate of $P^H$, given by (3.3). This has precisely the correct form in the sense that, as $\lambda$ is reduced, the two Prandtl–Hopkins points will approach the nip and collide to produce a stagnation point where

$$\overline{Z}/H_0 = \frac{1-S^{1/2}}{1+S^{1/2}} \tag{3.5}$$

which is consistent with (2.24), §2.

*The limit $S \to 0$*

In order to see how the recirculating flow develops as speed ratio tends to zero, figure 10(*a–e*) shows streamlines for $S = 0.8$, 0.5, 0.2, 0.05 and 0 with $R/H_0 = 100$, $Ca = 0.1$ and a flooded inlet (in the $S = 0$ case a contact angle of 30° is assumed based on experimental observation, Gaskell *et al.* 1998). What they reveal is a smooth transition to a single recirculation at $S = 0$. As $S \to 0$:

(i) the stagnation–saddle point $A^+$ approaches the upper cylinder and disappears (at $S = 0$) as the strength of the transfer jet diminishes to zero;

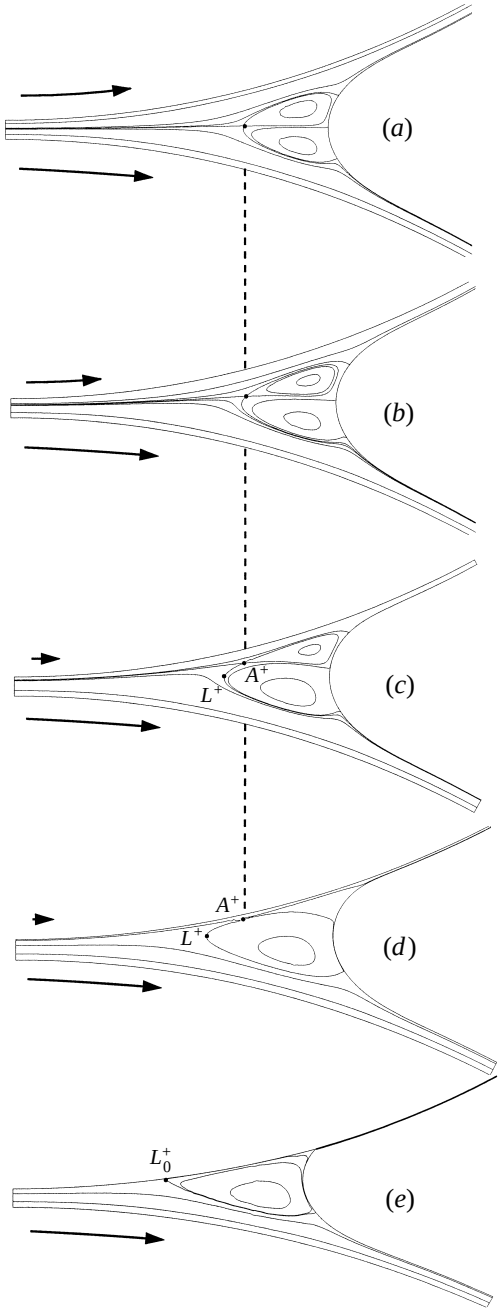


FIGURE 10. Downstream-only FE solutions for $Ca = 0.1$, $R/H_0 = 100$, $St = 0$, $R_1/R_2 = 1$ illustrating flow in the limit $S \to 0$: (*a*) $S = 0.8$; (*b*) 0.5; (*c*) 0.2; (*d*) 0.05; (*e*) 0.

(ii) $L^+ \to L_0^+$ ($P^H \to L_0^+$), where $L_0^+$ is the separation point on the stationary cylinder at a distance $[(3\lambda - 2)RH_0]^{1/2}$ from the nip (via the Prandtl–Hopkins conditions).

### 3.3. *Eddy structure: flow topology and flow patterns*

The aim of this section is to explore the range of possible flow patterns in the recirculating flow with $\lambda > \bar{\lambda}(S)$. These will depend on where the stagnation–saddle

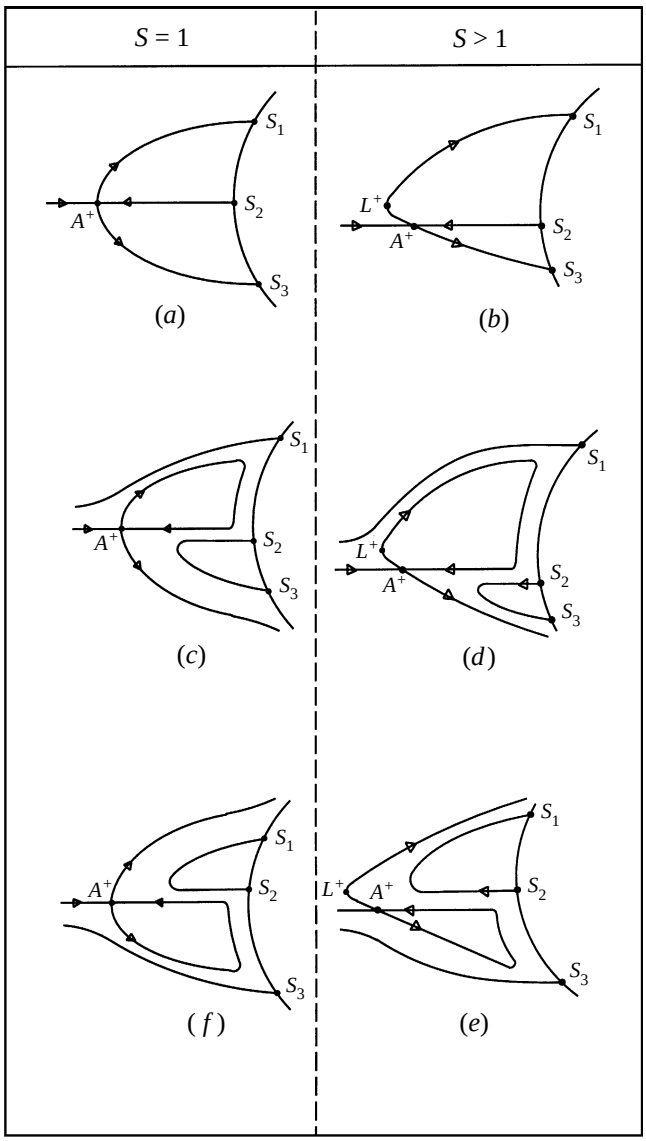


FIGURE 11. Flow patterns in the downstream recirculation region for both $S = 1$ and $S \neq 1$ ($S > 1$). There are five different patterns: (*a,b*) are of the joint eddy type and (*c–f*) are of the disjoint eddy type featuring a transfer jet.

points are located and how their insets and outsets are connected. In the particular case of fully submerged cylinders, the recirculations extend to 'infinity', figure 2(*a,c*), and the 'free' insets/outsets at $A^+$ and $A^-$ remain unconnected. With recirculations of finite extent, bounded for example by an interface (figures 1*a*, 1*b*, 2*b*, 2*d*) the flow patterns are quite different and the saddle points may or may not exist depending on $\lambda$, figure 6, or $Ca$ – see §3.5. Here it is assumed that $A^+$ exists as an interior point between the nip and the interface – with one inset extending upstream of the nip. As for the remaining inset and two outsets, they are able to connect in three different ways – for both $S = 1$ and $S \neq 1$ as illustrated in figure 11(*a–f*). It is sufficient to consider $S > 1$ only since $S < 1$ gives the same set of flow patterns.

| | Flow pattern | Flow topology |
|---|---|---|
| (A) | $S = 1$; symmetric flow with no transfer jet, $L^+$ and $A^+$ coincident. | joint eddy |
| (B) | $S \neq 1$; asymmetric flow with no transfer jet, $L^+$ lies between $A^+$ and the faster moving cylinder. | joint eddy |
| (C) | $S = 1$; asymmetric flow with a transfer jet, $L^+$ and $A^+$ coincident. | disjoint eddy |
| (D) | $S \neq 1$; asymmetric flow with a transfer jet directed from fast to slow moving cylinder; $L^+$ connected to homoclinic orbit through $A^+$. | disjoint eddy |
| (E) | $S \neq 1$; asymmetric flow with a transfer jet directed from slow to fast moving cylinder. $L^+$ not connected to homoclinic orbit through $A^+$. | disjoint eddy |

TABLE 2. Possible flow patterns and topologies.

In the first case, figure 11(*a,b*) the inset and two outsets connect to stagnation points $S_1$, $S_2$ and $S_3$ on the interface. The local flow structure, close to $A^+$, can be inferred by knowing the positions across the gap at $X = A$ where $u = 0$. It follows via equations (2.8) and (2.26) that these positions are $Z = 0$ and $Z/H(A) = (1 - S)/(1 + S)$. They are coincident when $S = 1$, figure 11(*a*); otherwise a recirculation (with $u = 0$ at $(X, Z) = (A, 0)$) lies above $A^+$ when $S > 1$ (and below $A^+$ when $S < 1$) as indicated in figure 11(*b*). Wicks *et al.* (1995) examined the special case $S = 1$ and referred to this as a 'joint eddy topology'. Its key feature is the presence of two eddies attached to the interface and sharing a common streamline. Clearly this joint eddy topology exhibits two different flow patterns, figures 11(*a*) and 11(*b*), corresponding to:

(A) symmetric flow, $S = 1$ with $L^+$ and $A^+$ coincident;

(B) asymmetric flow, $S \neq 1$ ($S > 1$) in which $L^+$ lies between $A^+$ and the faster moving cylinder.

In the second (and third) case, figures 11(*c,d*) and 11(*e,f*) the inset at $A^+$ connects with the upper (lower) of the two outsets respectively to establish an interior eddy bounded by a homoclinic orbit. The remaining outset exits with the outflow. In all four schematics the flow topology is the same in that the eddies are now separated with only one attached to the interface. Again using the terminology of Wicks *et al.* (1995), this is referred to as a 'disjoint eddy topology' and its key feature is the presence of a transfer jet or meandering streamtube carrying fluid across the recirculation region. The transfer jet is directed from the upper to the lower cylinder in figure 11(*c,d*) and from the lower to the upper in figure 11(*e,f*). However flow patterns 11(*c*) and 11(*f*) are identical and hence there are three different flow patterns, figure 11(*c*), 11(*d*) and 11(*e*) corresponding to:

(C) $S = 1$ with $L^+$ and $A^+$ coincident;

(D) $S \neq 1$ with $L^+$ connected to the homoclinic orbit;

(E) $S \neq 1$ with $L^+$ not connected to the homoclinic orbit.

The five flow patterns (A)–(E) exhibiting the two flow topologies are summarized in table 2.

### 3.4. *Eddy structure: transfer jets*

Known mechanisms for generating transfer jets include (i) unequal cylinder speeds, $S \neq 1$, (ii) unequal cylinder radii, $R_1 \neq R_2$, (iii) gravity acting across the gap. Consider each in turn:

(i) $S > 1$ ($S < 1$), $R_1 = R_2$ and cylinders side by side as in figure 1(*a*). Flow is of the disjoint eddy type with a transfer jet which, experiment suggests (Gaskell *et al.* 1998)

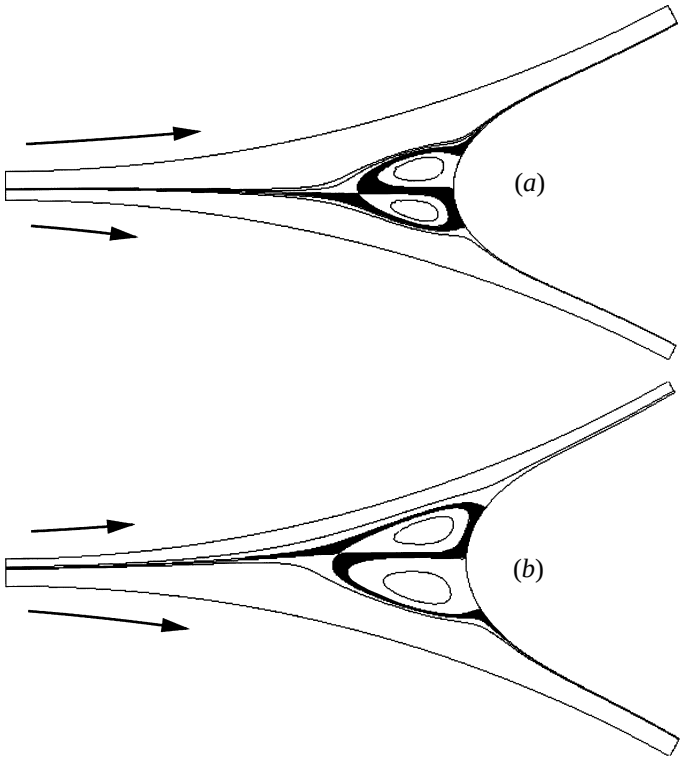


FIGURE 12. FE solutions for flow downstream of the nip in the absence of gravity $St = 0$, $R_1/R_2 = 1$, $R/H_0 = 100$, $Ca = 0.1$ for (*a*) $S > 1$, (*b*) $S < 1$ illustrating the presence of a transfer jet (shaded) taking fluid from the slower to the faster moving cylinder.

and FE calculations confirm, transfers fluid from the slower to the faster moving cylinder – see figure 12(*a,b*) for $S > 1$ and $S < 1$ respectively. These correspond to flow pattern (E), schematic 11(*e*).

(ii) $S = 1$, $R_1 \neq R_2$ and cylinders side by side as in figure 1(*a*). Again flow is of the disjoint eddy type – with flow pattern (C) – as illustrated in schematic 11(*c*). Experimental results and FE calculations confirm that the transfer jet is extremely weak and transfers fluid from the cylinder of small radius to that of larger radius, figure 13(*a*).

(iii) $S = 1$, $R_1 = R_2$ and cylinders one above the other as in figure 1(*b*). Here gravity has only a hydrostatic effect in the interior of the flow yet it causes an asymmetric effect close to the downstream interface in the form of a transfer jet taking fluid in the direction in which gravity acts. This corresponds to flow pattern (C), see figure 13(*b*) and schematic 11(*c*).

There is a fourth mechanism for generating transfer jets, which appears in the upstream recirculation region due to an 'asymmetric inlet feed'. Upstream of the nip, where $A^-$ is an interior stagnation–saddle point the disjoint eddy topology can be identified in figure 14 which is a FE solution for the full flow field. The transfer jet is directed from the lower to upper cylinder, regardless of cylinder speeds, radii or whether gravity is present/absent. Here $S = 1$ and the inlet is asymmetrically fed via an inlet film attached to the lower cylinder and the primary requirement is to transfer fluid to the upper cylinder.

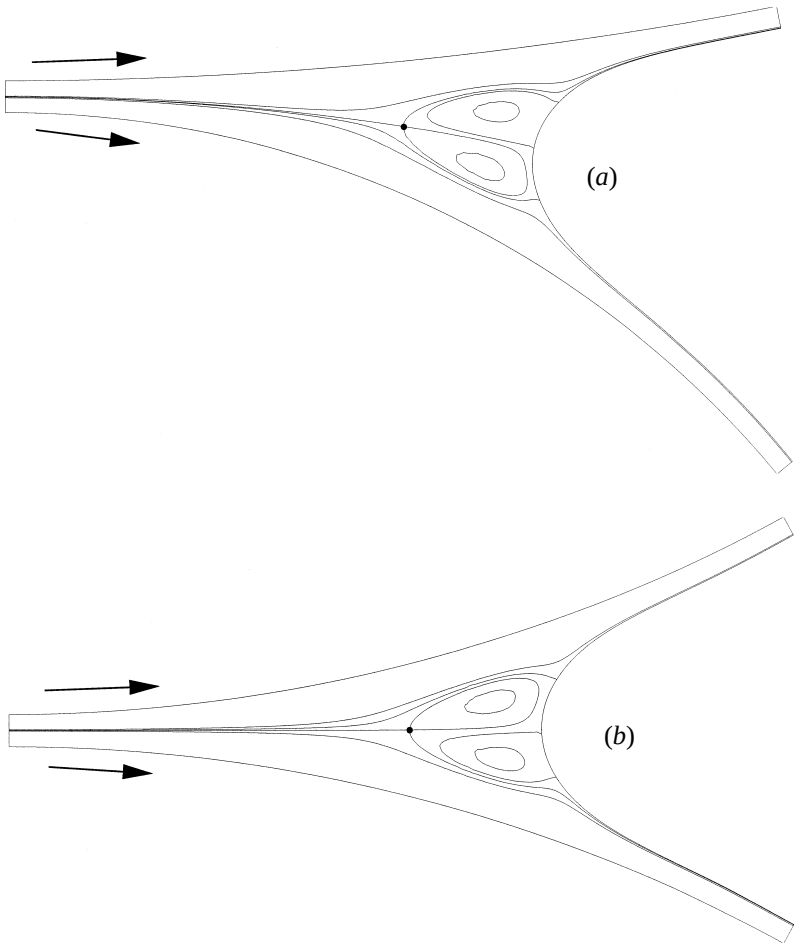


FIGURE 13. Downstream-only FE solutions for $S = 1$, $Ca = 0.1$, $R/H_0 = 100$: (*a*) $St = 0$, $R_1/R_2 = 4$, showing a transfer jet from the smaller to the larger radius cylinder; (*b*) $St = 0.01$, $R_1/R_2 = 1$ showing a gravitational transfer jet. $A^+$ is indicated by •.

There is also the question of the circumstances in which the joint eddy topology of schematic 11(*b*) – flow pattern (B) – might occur in practice? Clearly it will arise when two competing, asymmetric effects are in balance; for example when one due to unequal speeds is balanced by another due to gravity or unequal cylinder radii. Figures 15(*a,b*) shows computational flow fields for $S \neq 1$ with two competing effects in balance such that no transfer jet exists and the flow structure in the recirculation region corresponds to schematic 11(*b*). Figure 15(*c*) illustrates the joint eddy topology for $S = 1$ in which asymmetric effects due to gravity and unequal cylinder radii are in balance, schematic 11(*a*).

Finally, flow pattern (D), schematic 11(*d*) refers to flows with two competing asymmetric effects which are not in balance. One, due to unequal cylinder speeds, is weaker than another due, for example, to gravity or unequal cylinder radii and – as a consequence – the transfer jet is directed from the faster to the slower moving cylinder.

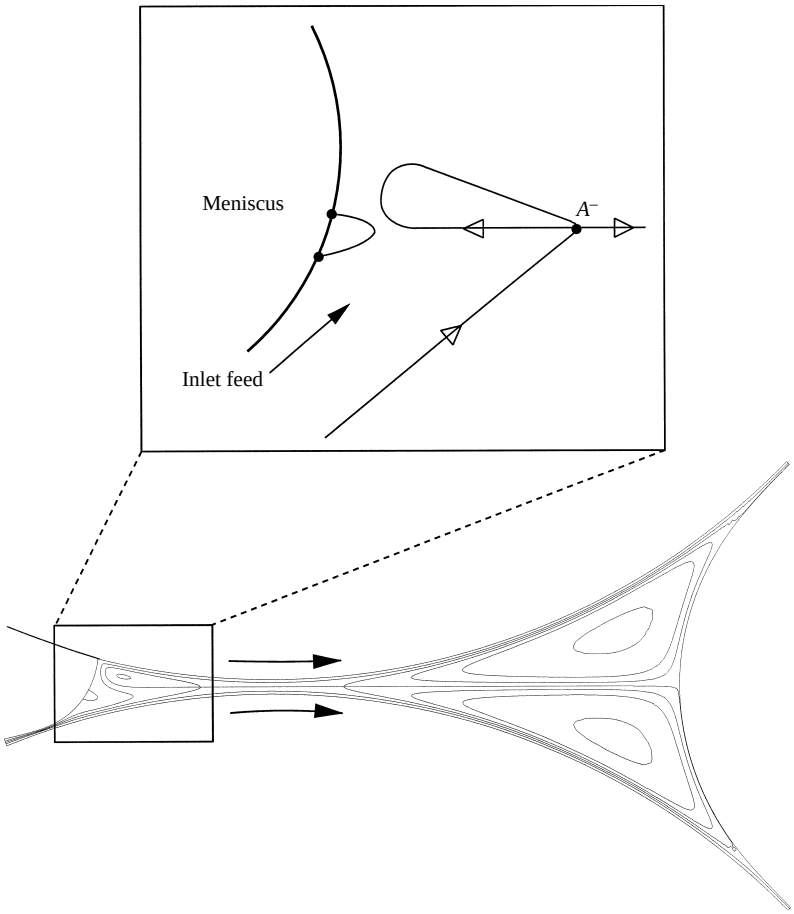


FIGURE 14. FE solution for $S = 1$, $Ca = 0.0015$, $R/H_0 = 100$, $St = 0$, $R_1/R_2 = 1$ showing the upstream disjoint eddy flow caused by the inlet feed condition.

### 3.5. *Effect of capillary number*

FE computations by Coyle *et al.* (1986) revealed that the major effect of $Ca$ is on the location of the downstream meniscus and the extent of the recirculations. As $Ca$ is increased for the case $S = 1$ they showed that the two recirculations contract and then disappear as $A^+$ approaches and then coincides with the stagnation point $S_2$ on the interface, see schematic 11(*a*).

In order to examine the effect that the meniscus approaching the nip has on flow structure for asymmetric flow, FE solutions are considered for $S = 0.1$, $R/H_0 = 100$ as shown in figure 16(*a–d*). As $Ca$ is increased beyond the value 0.2, figure 16(*a*), the disjoint eddy structure contracts, figure 16(*b*), and the 'initially large', attached eddy, disappears leaving the stagnation–saddle point $A^+$ with its homoclinic orbit, figure 16(*c*), $Ca = 0.42$. As $Ca$ is further increased $A^+$ is then annihilated via a saddle–node bifurcation leaving only a dividing streamline with a stagnation point $S_1$ on the interface, figure 16(*d*).

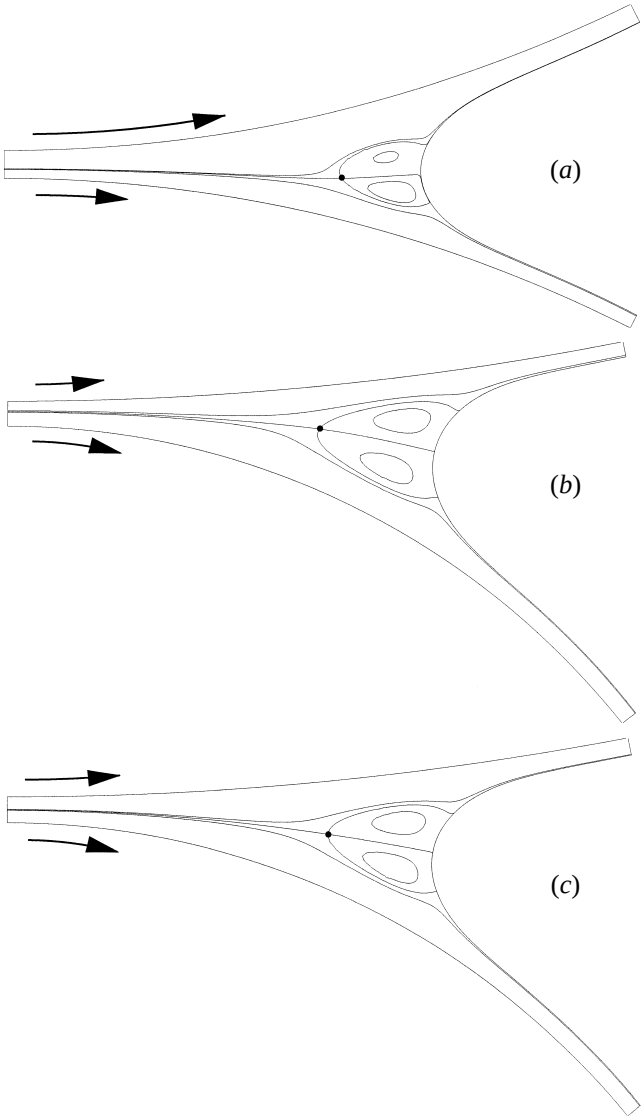


FIGURE 15. Downstream-only FE solutions for $Ca = 0.1$, $R/H_0 = 100$. In each case two transfer jets are in balance: due to (*a*) gravity and unequal speeds, $S = 2$, $St = 0.03$, $R_1/R_2 = 1$; (*b*) unequal speed and unequal radii, $S = 0.69$, $St = 0$, $R_1/R_2 = 4$; (*c*) gravity and unequal radii, $S = 1$, $St = 0.007$, $R_1/R_2 = 4$. $A^+$ is indicated by •.

## 4. Film thicknesses $H_1$, $H_2$

With $\theta$ given by (2.26), the $Z$-coordinate of the stagnation–saddle point $A^+$ is known and so the flux of fluid passing above and below is readily determined. Provided the transfer jet is weak, so that the flux transferred in this way can be assumed to be negligible, fluid will emerge in uniform layers of thickness $H_1$ and $H_2$ given by

$$U_1H_1 = \int_{\theta H(A)}^{H(A)} U\,\mathrm{d}Z, \quad U_2H_2 = \int_0^{\theta H(A)} U\,\mathrm{d}Z. \tag{4.1}$$

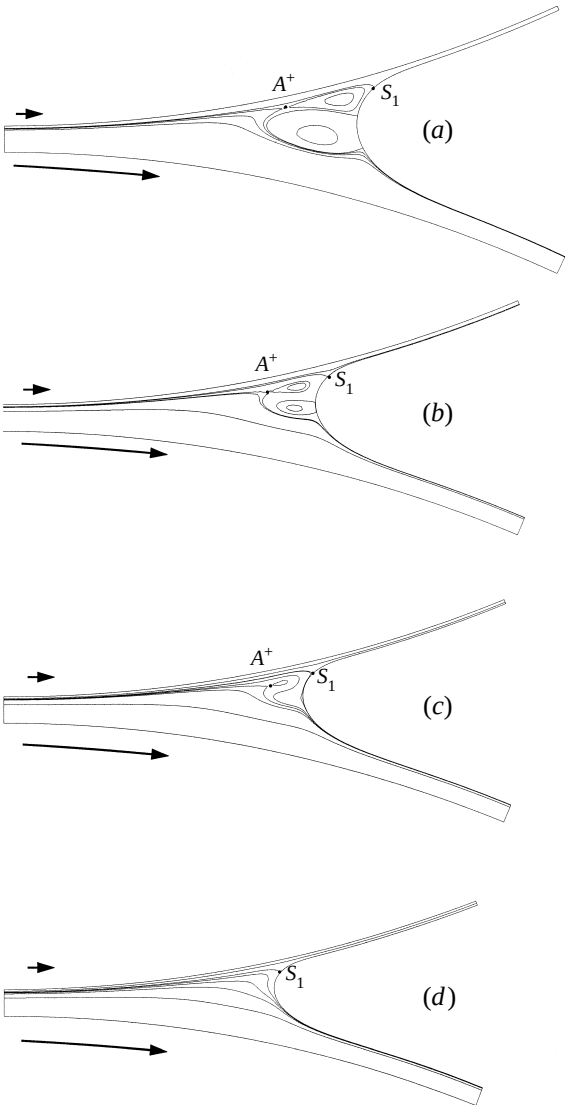


FIGURE 16. Downstream-only FE solutions for $S = 0.1$, $R/H_0 = 100$, $St = 0$ and $R_1/R_2 = 1$ showing the effect of $Ca$ on the downstream disjoint eddy flow: (*a*) $Ca = 0.2$ with two eddies in the recirculation region; (*b*) $Ca = 0.35$ with a reduced attached eddy; (*c*) $Ca = 0.42$ where the large 'attached eddy' has disappeared due to the meniscus advancing towards $A^+$ (indicated by •); (*d*) $Ca = 0.7$ where the meniscus continues to advance and $A^+$ disappears as a result of a saddle–node annihilation. A dividing streamline connects with the meniscus at $S_1$.

It then follows that

$$\frac{H_1}{H(A)} = \frac{S(S+3)}{6(1+S)^2}, \quad \frac{H_2}{H(A)} = \frac{(1+3S)}{6(1+S)^2}, \tag{4.2}$$

and

$$\frac{H_1}{H_2} = \frac{S(S+3)}{(1+3S)}. \tag{4.3}$$

In the light of the $S^{0.65}$ power law reported by Benkreira *et al.* (1981) and Coyle *et al.* (1986) one might perhaps have expected the analysis to reveal an $S^{2/3}$ power

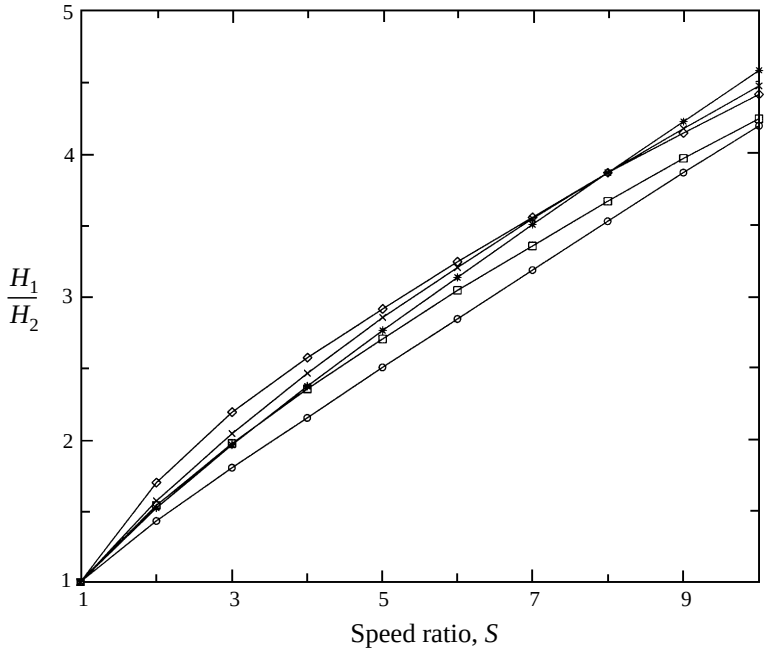


FIGURE 17. Film thickness ratio $H_1/H_2$ as a function of $S$, $R_1/R_2 = 1$: expression (4.3) ($\circ$); FE results obtained for $Ca = 0.01$ ($\diamond$), 0.1 ($\square$), 0.5 ($*$) and for comparison $S^{0.65}$ ($\times$).

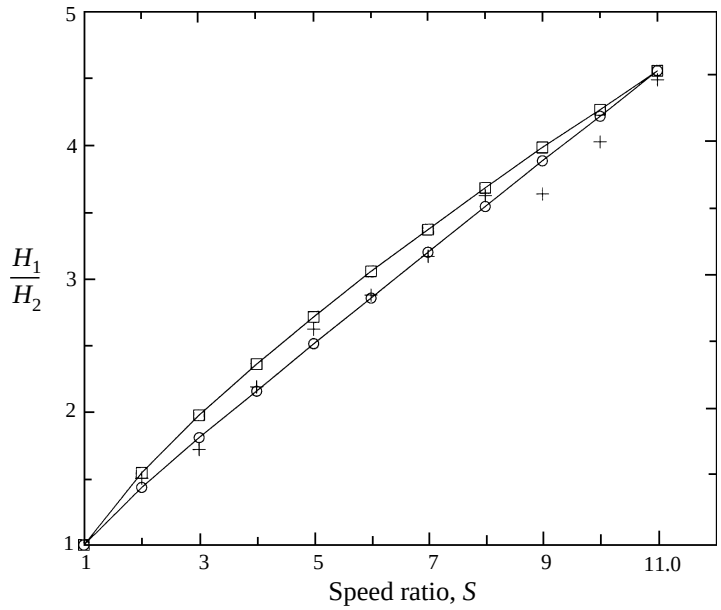


FIGURE 18. Film thickness ratio as a function of $S$, $R_1/R_2 = 1$. A comparison of analytical, expression (4.3) ($\circ$) and FE, $Ca = 0.1$ ($\square$), predictions with experimental data ($+$) (Gaskell *et al.* (1998).

law for $H_1/H_2$ as opposed to the algebraic expression (4.3). Figure 17 compares predictions for film thickness ratio given by this expression with the $S^{0.65}$ power law and FE computations for flooded inlets for three values of $Ca$, 0.01, 0.1 and 0.5 with $S \in [1, 10]$. It is observed that over this range of $S$ expression (4.3) consistently under-predicts $H_1/H_2$. This is expected due to the neglect of the weak transfer jet which has the effect of increasing $H_1$ at the expense of $H_2$. The FE results also indicate a slight dependence on $Ca$ which again is not surprising since $Ca$ controls the extent of the recirculation region from the stagnation–saddle point to the downstream meniscus.

Figure 18 compares analytical and numerical predictions for $H_1/H_2$ with recent experimental data collected from a high-precision, laboratory-scale apparatus having horizontally-aligned cylinders, Gaskell *et al.* (1998). Film thicknesses were measured with a maximum error of 5% and like those of Benkreira *et al.* (1981), where cylinders were aligned vertically, are in close accord with the theoretical predictions.

Finally, a feature of (4.3) is its range of applicability. It was first derived by Savage (1992) for flooded inlets and cylinders of equal radius yet the only essential requirement is the presence of a region of quasi-unidirectional flow terminated by a stagnation–saddle point. It therefore applies to both fully flooded and moderately starved inlets with non-dimensional flow rates $\lambda \in [1/3, \lambda_{max}]$.

## Appendix. Stagnation points in the flow between cylinders of unequal radii, $R_1$ and $R_2$

Adopting the same scalings as those given in (2.3) and with $\delta$ and $R$ as defined in §2, the upper and lower cylinder surfaces are given by

$$\left.\begin{aligned} H_1(X) &= H_0 + \frac{X^2}{2R_1} = H_0\left(1 + x^2\frac{R}{R_1}\right) = H_0\eta_1(x), \\ H_2(X) &= H_0 + \frac{X^2}{2R_2} = H_0\left(1 + x^2\frac{R}{R_2}\right) = H_0\eta_2(x). \end{aligned}\right\} \tag{A 1}$$

The dependent variables are expanded in powers of $\delta^2$ and the zero-order solution for $u(x, z)$ satisfying $u = 1$ on $z = -\eta_2(x)$ and $u = S$ on $z = \eta_1(x)$ is

$$u(x,z) = S + \frac{(S-1)}{2}\left(\frac{z}{\eta}\right) - \frac{(S-1)}{2}\left(\frac{\eta_1}{\eta}\right) + \frac{p_x}{2}(z-\eta_1)(z+\eta_2). \tag{A 2}$$

Similarly the solution for $w(x, z)$ satisfying

$$\left.\begin{aligned} w &= -\frac{\mathrm{d}\eta_2}{\mathrm{d}x} = -\eta_{2x} \quad \text{on} \quad z = -\eta_2(x), \\ w &= S\frac{\mathrm{d}\eta_1}{\mathrm{d}x} = S\eta_{1x} \quad \text{on} \quad z = +\eta_1(x), \end{aligned}\right\} \tag{A 3}$$

is given by

$$\begin{aligned} w = {} & (S-1)(z^2-\eta_2^2)\left(\frac{\eta_x}{4\eta^2}\right) + \frac{1}{2}\left(\frac{\eta_2}{\eta}\right)_x(1-S)(z+\eta_2) - \eta_{2x} \\ & -\frac{p_{xx}}{2}\left(\frac{z^3+\eta_2^3}{3} + \frac{(\eta_2-\eta_1)}{2}(z^2-\eta_2^2) - \eta_2\eta_1(z+\eta_2)\right) \\ & -\frac{p_x}{2}\left(\frac{(\eta_{2x}-\eta_{1x})}{2}(z^2-\eta_2^2) - (\eta_2\eta_{1x}+\eta_1\eta_{2x})(z+\eta_2)\right). \end{aligned} \tag{A 4}$$

Using the Reynolds equation to eliminate $p_{xx}$ yields

$$w(x,z) = (S-1)(z^2-\eta_2^2)\left(\frac{\eta_x}{4\eta^2}\right) + \frac{1}{2}\left(\frac{\eta_2}{\eta}\right)_x (1-S)(z+\eta_2) - \eta_{2x} + \frac{1}{2}\left(\frac{3\eta_x}{\eta}p_x - \frac{3}{2}\frac{\eta_x}{\eta^3}(1+S)\right)\left(\frac{z^3+\eta_2^3}{3} + \frac{(\eta_2-\eta_1)}{2}(z^2-\eta_2^2) - \eta_2\eta_1(z+\eta_2)\right) - \frac{p_x}{2}\left(\frac{(\eta_{2x}-\eta_{1x})}{2}(z^2-\eta_2^2) - (\eta_2\eta_{1x}+\eta_1\eta_{2x})(z+\eta_2)\right). \tag{A 5}$$

Denoting the coordinates of a stagnation point by

$$\left.\begin{array}{ll} X = A, & Z = -H_2(A) + 2\gamma H(A), \\ x = a, & z = -\eta_2 + 2\gamma\eta, \end{array}\right\} \tag{A 6}$$

where $H_1(X) + H_2(X) = 2H(X)$ and $\eta_1(x) + \eta_2(x) = 2\eta(x)$. Then $u = w = 0$ yields

$$0 = 1 + (S-1)\gamma + 2p_x\eta^2\gamma(\gamma-1), \tag{A 7}$$

$$0 = (S-1)\left(\frac{\eta_x}{\eta^2}\right)(\eta^2\gamma^2 - \eta\eta_2\gamma) + \left(\eta_{2x} - \frac{\eta_2\eta_x}{\eta}\right)(1-S)\gamma - \eta_{2x} + 3\eta_x\left(p_x - \frac{(1+S)}{2\eta^2}\right)\left(\frac{3\eta_2^2\gamma + 4\eta^2\gamma^3 - 6\eta_2\eta\gamma^2}{3} + (\eta_2-\eta_1)(\eta\gamma^2 - \eta_2\gamma) - \eta_2\eta_1\gamma\right). \tag{A 8}$$

With $p_x\eta^2/(1+S)$ replaced by $\alpha$, then after some manipulation (A 7) and (A 8) reduce to two equations for $\alpha$ and $\gamma$:

$$0 = \left(\frac{1}{1+S}\right) + \left(\frac{S-1}{1+S}\right)\gamma + 2\alpha\gamma(\gamma-1), \tag{A 9}$$

$$0 = \eta_{2x}((1-S)\gamma - 1 - 2\alpha(1+S)\gamma(\gamma-1)) + \eta_x\left(\frac{(S-1)}{(1+S)^2}\gamma^2 + 2\alpha\gamma^2 + 2\gamma^2 + (2\alpha-1)(2\gamma^3 - 3\gamma^2)\right). \tag{A 10}$$

The coefficient of $\eta_{2x}$ is identically equal to zero by way of (A 9), hence (A 9) and (A 10) reduce to a cubic equation in $\gamma$:

$$\gamma(\gamma-1)\left(\gamma - \frac{1}{1+S}\right) = 0. \tag{A 11}$$

As mentioned in §2, $\gamma = 0$ and $\gamma = 1$ are special cases corresponding to $S = \infty$ and $S = 0$ which need to be considered separately. The remaining solution is

$$\gamma = \frac{1}{1+S} \quad \text{and} \quad \alpha = 1, \quad \text{that is} \quad p_x = \frac{1+S}{\eta^2}. \tag{A 12}$$

This refers to a stagnation point at $(X, Z) = (A, -H_2 + 2\gamma H)$ where

$$\frac{\mathrm{d}P}{\mathrm{d}X} = \frac{\mu(U_1+U_2)}{H^2(A)}, \tag{A 13}$$

and this point divides the gap (of width $2H(A)$) in the ratio

$$\frac{2H - 2\gamma H}{2H} = S = \frac{U_1}{U_2}. \tag{A 14}$$

## REFERENCES


Ballal, B. Y. & Rivlin, R. S. 1976 Flow of a Newtonian fluid between eccentric rotating cylinders: inertial effects. *Arch. Rat. Mech. Anal.* **62**, 237–294.

Benkreira, H., Edwards, M. F. & Wilkinson, W. L. 1981 Roll coating of purely viscous liquids. *Chem. Engng Sci.* **36**, 429–434.

Coyle, D. J., Macosko, C. W. & Scriven, L. E. 1986 Film-splitting flows in forward roll coating. *J. Fluid Mech.* **171**, 183–207.

Coyne, J. C. & Elrod, H. G. 1970 Conditions for the rupture of a lubricating film. Part I: theoretical model. *J. Lub. Technol.* **92**, 451–456.

Decré, M., Gailly, E., Buchlin, J.-M. 1995 Meniscus shape experiments in forward roll coating. *Phys. Fluids* **7**, 458–467.

Gaskell, P. H., Savage, M. D., Summers, J. L. & Thompson, H. M. 1995*a* Modelling and analysis of meniscus coating. *J. Fluid Mech.* **298**, 113–137.

Gaskell, P. H., Savage, M. D., Summers, J. L. & Thompson, H. M. 1995*b* Flow topology and transformation in a fixed-gap symmetric forward roll coating system. *Proc. 9th Intl Conf. Numerical Methods in Laminar and Turbulent Flow, Atlanta* (ed. C. Taylor & P. Durbetaki), pp. 984–995. Pineridge Press.

Gaskell, P. H., Savage, M. D. & Walker, D. J. 1998 An experimental investigation of asymmetric transfer jets, film-splitting and flow rates in roll coating. *Phys. Fluids*, in preparation,

Greener, J. & Middleman, S. 1975 A theory of roll coating of viscous and viscoelastic fluids. *Poly. Engng. Sci.* **15**, 1–10.

Greener, J. & Middleman, S. 1979 Theoretical and experimental studies of the fluid dynamics of a two-roll coater. *Ind. Engng Chem. Fundam.* **18**, 35–41.

Hintermaier, J. C. & White, R. E. 1965 The splitting of a water film between rotating rolls. *TAPPI J.* **48**, 617–625.

Jeffery, G. B. 1922 The rotation of two cylinders in a viscous liquid. *Phil. Trans. Roy. Soc. Lond.* A **101**, 169–174.

Kistler, S. F. & Scriven, L. E. 1983 Coating flows. In *Computational Analysis of Polymer Processing* (ed. J. R. A. Pearson & S. M. Richardson), pp. 243–299. Appl. Sci. Publishers.

Malone, B. 1992 An experimental investigation of roll coating phenomena. PhD thesis, University of Leeds.

Pitts, E. & Greiller, J. 1961 The flow of thin liquid films between rollers. *J. Fluid Mech.* **11**, 33–50.

Ruschak, K. J. 1982 Boundary conditions at a liquid/air interface in lubrication flows. *J. Fluid Mech.* **119**, 107–120.

Savage, M. D. 1982 Mathematical models for coating processes. *J. Fluid Mech.* **117**, 443–455.

Savage, M. D. 1992 The relevance of lubrication theory to roll coating. *AIChE Spring National Meeting, New Orleans, Paper* 39e.

Schneider, G. B. 1962 Analysis of forces causing flow in roll coaters. *Trans. Soc. Rheo.* **6**, 209–221.

Taylor, G. I. 1963 Cavitation of a viscous fluid in narrow passages. *J. Fluid Mech.* **16**, 595–619.

Thompson, H. M. 1992 A theoretical investigation of roll coating phenomena. PhD thesis, University of Leeds.

Van de Bergh, H. J. 1974 A study of cavitation for a cylinder sliding against a plate. MSc thesis, University of Leeds.

Wicks, P. J., Decré, M., Planquart, Ph. & Buchlin, J. M. 1995 Flow topology associated with different disjoint eddies in an asymmetric film-splitting problem. *Phys. Rev.* E **52**, 1281–1284.